GEOPHYSICAL RESEARCH LETTERS, VOL. 40, 778–784, doi:10.1002/GRL.50110, 2013

On the radiative forcing of contrail cirrus contaminated by black carbon

K. N. Liou,[1] Y. Takano,[1] Q. Yue,[1] and P. Yang[2]

Received 3 October 2012; revised 11 December 2012; accepted 20 December 2012; published 27 February 2013.

[1] The effects of internal and external mixings of black carbon (BC) (soot) in ice particles on the radiative properties of contrail cirrus are investigated using a simple ice plate model. The internal mixing state absorbs substantially more radiation as compared with its external mixing counterpart due to light absorption enhancement from all directions. The soot absorption effect is largely confined to wavelengths shorter than about 1.4 μm, beyond which ice absorption predominates. For an ice crystal size of 5 μm internally mixed with a soot particle of 0.1 μm radius in contrail cirrus with an optical depth of 0.5, the instantaneous radiative forcings at the top of and within the atmosphere are approximately 0.2 and 0.8 W/m^2, respectively. In view of the likelihood of multiple inclusions of soot particles in contrail cirrus, these values are lower limits. Thus, a realistic assessment of the global and regional radiative forcings of contrail cirrus for climate studies must account for the radiative effect induced by soot mixing states associated with the microscopic formation of ice particles. **Citation:** Liou, K. N., Y. Takano, Q. Yue, and P. Yang (2013), On the radiative forcing of contrail cirrus contaminated by black carbon, *Geophys. Res. Lett.*, *40*, 778–784, doi:10.1002/grl.50110.

1. Introduction

[2] Contrails or condensation trails are the upper ice crystal clouds produced by jet aircraft. They are visible line clouds generated by water vapor emissions that form behind an aircraft flying in sufficiently cold air. These ice clouds have been known to form through the freezing processes involving water droplets that are formed *a priori* on the soot (black carbon or BC) and sulfuric acid particles emitted from aircraft and/or background aerosol particles. In ice-supersaturated air masses, so-called persistent contrails frequently develop into more extensive contrail cirrus. Additionally, contrails may enhance extension of the natural cirrus cover in adjacent areas where relative humidity is too low for the spontaneous nucleation of ice crystals, an important indirect effect yet to be quantified.

[1]Joint Institute for Regional Earth System Science and Engineering, and Department of Atmospheric and Oceanic Sciences, University of California, Los Angeles, CA 90095, USA.
[2]Department of Atmospheric Sciences, Texas A&M University, College Station, TX 77845, USA.

Corresponding author: Y. Takano, Joint Institute for Regional Earth System Science and Engineering, and Department of Atmospheric and Oceanic Sciences, University of California, Los Angeles, CA 90095, USA. (ytakano@atmos.ucla.edu)

©2013. American Geophysical Union. All Rights Reserved.
0094-8276/13/10.1002/grl.50110

[3] On the basis of available measurements, aircraft emit about 10^{15} soot particles larger than about 5 nm/kg of burnt fuel (~0.01–0.2 g soot/kg fuel) with concentration exceeding 10^6/cm^3 near the engine exit plane [*Petzold and Döpelheuer*, 1998]. Agglomerated soot particle sizes are typically 10–100 nm. *Petzold et al*. [1999] showed that there exists a coagulated mode whose modal diameter is ~200 nm. The number of ice particles found in aged contrails correlates with the amount of absorbing material measured and air traffic density, revealing that a relationship exists between contrail ice particles and soot emission [*Ström and Ohlsson*, 1998]. *Schumann et al*. [2002] studied the impact of aircraft-emitted soot particles on contrail formation. In addition, homogeneous phase transitions could also lead to the formation of ice particles. Based on theoretical analysis and experimental results, pure liquid droplets formed from homogeneous nucleation (smaller than 5 μm) can freeze spontaneously at temperatures below −40°C. Consequently, most of the contrail particles are internally contaminated by soot particles.

[4] Understanding the radiative forcing of contrail cirrus requires both fundamental knowledge and reliable data concerning its scattering and absorption properties. However, the contamination of ice particles by means of internal mixing, in which soot particles serve as nuclei, has not been accounted for in the radiative forcing analysis. This paper presents some computational results to illustrate the significance of "dirty" contrail ice particles on the radiative forcing calculations. In section 2, we present the solar single-scattering properties of pure ice, and ice contaminated by soot externally and internally, using the hexagonal plate as the prototype in the computation. We have also developed parameterizations of the spectral extinction coefficient, single-scattering co-albedo, and asymmetry factor for contrail ice particles for efficient application to radiative transfer calculations. Results of the radiative forcing analysis are presented in section 3, including a discussion on the importance of soot contamination. Concluding remarks are given in section 4.

2. Computation of the Single-Scattering Properties of Contrail Ice Particles

[5] In a recent paper, *Yang et al*. [2013] presented a spectrally consistent database containing the scattering, absorption, and polarization properties of 11 randomly oriented ice crystal habits that range in size from 2 to 10,000 μm for wavelengths of 0.2-100 μm. This unified database represents a substantial improvement upon the previous databases published in *Yang et al*. [2000] for the solar spectrum (0.2-5 μm) and *Yang et al*. [2005] for the thermal infrared spectrum (5-100 μm). It also bridges gaps in spectral resolutions and provides improved calculations for small ice crystal size parameters, as well as

information relating to the volume and projected area of each habit. We have adopted this database in the solar spectrum to obtain the single-scattering properties in terms of the extinction coefficient, single-scattering albedo, and asymmetry factor for the condition of pure ice. To simplify and focus our objective to investigate the effect of soot on the radiative forcing of contrail cirrus, we have selected a simple and representative shape -namely, hexagonal plate- for our study. Computations of the single-scattering properties of ice crystals have been well-known in the field and we have cited relevant papers above.

[6] To characterize the ice crystal size distribution and account for the habit factor for radiative transfer calculations, we have defined a mean effective size as the ratio of ensemble particle volume and the particle projected area as follows [*Liou et al*., 2008]:

$$De = \int V(L)n(L)dL \Big/ \int A(L)\, n(L)dL = \mathrm{IWC}/\left[\rho_i \int A(L)\, n(L)dL\right] = \mathrm{IWC}/\rho_i A_c, \quad (1)$$

where we may insert a factor of 3/2 for consistent comparison with the definition of spherical particles, $V(L)$ and $A(L)$ are the volume and projected area, respectively, of an ice crystal with a maximum dimension L, $n(L)\,dL$ denotes the number density of ice crystals in the size interval (L, $L+dL$), ρ_i is the ice density, A_c represents the total projected area for a given ice crystal size and habit distribution, and the ice water content (IWC) is defined as follows:

$$\mathrm{IWC} = \int V(L)\rho_i n(L)dL. \quad (2)$$

Figure 1 shows the spectral extinction coefficient, single-scattering co-albedo, and asymmetry factor as a function of wavelength from 0.2 to 5 μm for three mean effective sizes *De* of 5, 10, and 20 μm, representing contrail ice crystal sizes. The mean effective ice crystal sizes of 5 and 10 μm using the gamma function for size distributions developed in this study are in line with the value of about 6 μm suggested in *Iwabuchi et al*. [2012] and the sizes presented in *Liou et al*. [1998]. The spectral extinction coefficient (km^{-1}) when multiplied by the cloud thickness results in optical depth. We may also compute the averaged spectral extinction efficiency for randomly oriented ice crystals. For $De = 10$ and 20 μm, the average size parameter is sufficiently large in the visible and near-infrared wavelengths such that the averaged extinction efficiency is approximately equal to 2 on the basis of the optical theorem, except in the vicinity of about 3 μm where a significant dispersion of the real part of the refractive index for ice occurs. The minimum, shown at 2.85 μm, is referred to as the Christiansen effect [*Christiansen*, 1884, 1885], which occurs when the real part of the refractive index approaches 1, while the corresponding imaginary counterpart is substantially large, resulting in the domination of absorption. The single-scattering co-albedo pattern mimics variability of the imaginary refractive index for ice and generally increases with increasing wavelength. The maximum asymmetry factor values shown in the vicinity of 2.85 μm for the three mean effective sizes are related to the Christiansen effect, leading to sharp diffraction peaks in phase functions.

[7] For efficient computational purposes, we have carried out parameterization of the spectral single-scattering properties for contrail cirrus by employing the preceding database. Following *Liou et al*. [2008], the extinction coefficient, single-scattering co-albedo, and the first four Legendre expansion coefficients of the phase function for use in four-stream radiative transfer calculations can be expressed in the following polynomial forms:

$$\tau(\lambda) = \beta_e(\lambda)\Delta z = \mathrm{IWP}\sum_{n=0}^{N} a_n(\lambda)/De^n \quad (3)$$

$$1 - \varpi_0(\lambda) = \exp\left[\sum_{n=0}^{N} b_n(\lambda)De^n\right] \quad (4)$$

$$\varpi_i(\lambda) = \sum_{n=0}^{N} c_{ni}(\lambda)De^n, \quad i = 1-4 \quad (5)$$

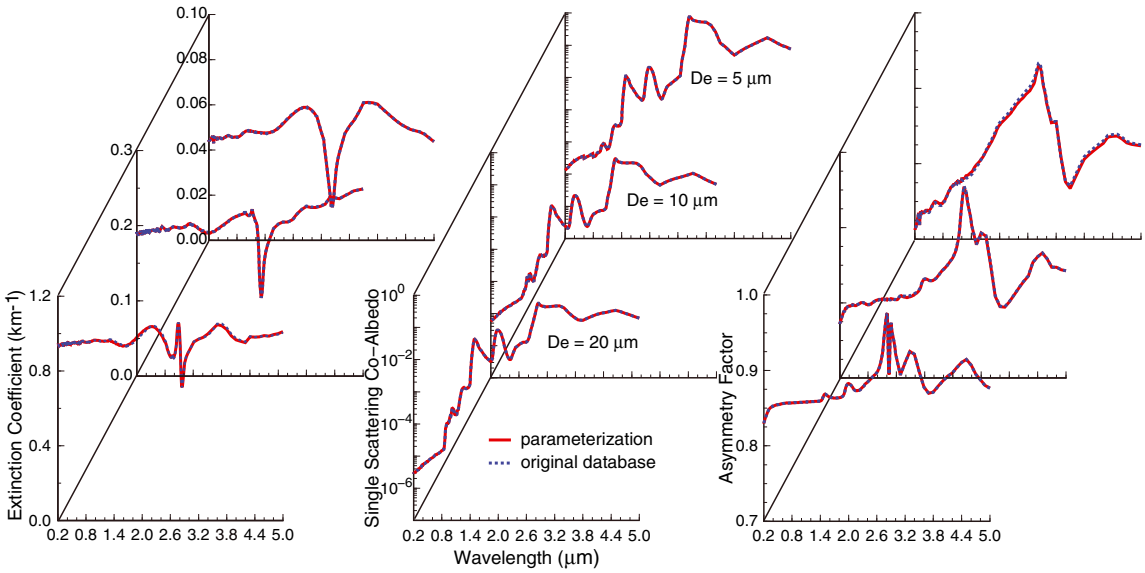

Figure 1. Spectral extinction coefficient, single-scattering co-albedo, and asymmetry factor as a function of wavelength from 0.2 to 5 μm for three mean effective ice crystal sizes of 5, 10, and 20 μm. The results are derived from the database developed by *Yang et al*. [2013]. Also shown are parameterization results based on equations (3–5).

where $\tau(\lambda)$ is the spectral optical depth, $\beta_e(\lambda)$ is the spectral extinction coefficient, Δz is the cloud thickness; IWP is the ice water path, the product of IWC and cloud thickness; and a_n, b_n, and c_{ni} are the fitting coefficients, which are functions of the wavelength. In order to achieve an accuracy within 0.1%, we set $N=6$. For the single-scattering co-albedo, we have used the logarithmic parameterization to represent extremely small values.

[8] For the cases involving pure ice crystals externally and internally contaminated by soot, conventional light-scattering methods such as those used for the construction of the database presented above cannot be applied. We have used the geometric-optics surface-wave (GOS) approach for the computation of light absorption and scattering by spherical and nonspherical particles for application to aggregates and snow grains with external and internal mixing structures developed by *Liou et al*. [2010, 2011]. In this theoretical development, the concept of adding the surface-wave contribution as a perturbation term to the geometric-optics core is followed, including Fresnel reflection-refraction and Fraunhofer diffraction. In the reflection and refraction components, the complex shape and composition can be accounted for by using the hit-and-miss Monte Carlo photon-tracing method. With reference to surface waves, a nonspherical correction factor was introduced using a nondimensional volume parameter. We cross-checked the single-scattering results for light scattering by columns and plates with the results computed from the rigorous finite difference time domain (FDTD) and discrete dipole approximation (DDA) methods. We demonstrated that the results for randomly oriented columns and plates evaluated from GOS are comparable to those derived from the FDTD and DDA counterparts for size parameters smaller than about 20, beyond which the rigorous numerical approaches are computationally unfeasible.

[9] We have performed calculations of the extinction coefficient, single-scattering albedo, and asymmetry factor for plate crystals with smooth and moderately rough surfaces externally and internally mixed with soot particles covering all the wavelengths employed in the database [*Yang et al*., 2013] and for maximum dimensions ranging from 2 to 404 μm. For sensitivity studies, we have selected two soot sizes: 0.1 and 0.5 μm. Soot particles at 0.1 μm that were used in this study are in line with those in observations [*Petzold et al*., 1998, Figure 1], and we have used 0.5 μm as the upper bound in the sensitivity study. We found that there are two sources of spectral index of refraction data for soot presented by *Krekov* [1993] and *d'Almeida et al*. [1991]. We have investigated the effect of the different index refraction sources on the computation of the spectral single-scattering properties. For all practical purposes, the resulting differences are indistinguishable. Moreover, soot contamination of pure ice crystals only affects the absorption properties of ice particles, while the extinction coefficient and asymmetry factor for these two cases are essentially the same as their pure ice counterparts. Also note that deviations of the single-scattering results for plate crystals with moderately rough surfaces from those for smooth plate crystals are insignificant.

[10] Figure 2 depicts the single-scattering co-albedo for pure ice, external mixing, and internal mixing as functions of wavelength from 0.2 to 5 μm for three *De* and two soot particle radii denoted by r_{soot}. Because variability in the real and imaginary parts of refractive indices for soot in the UV, visible, and near infrared is much smaller than those for pure ice, the spectral single-scattering co-albedo shows relative smooth patterns. The following general patterns are evident from the spectral results: (1) internal mixing cases absorb more light than their external mixing counterparts; (2) the effect of soot absorption on ice crystals is primarily confined to UV, visible, and near-infrared wavelengths, shorter than about 2.5 μm, beyond which ice absorption predominates; (3) for $r_{\text{soot}}=0.1$ μm, a typical size of soot particle, the single-scattering co-albedo increases by more than a factor of 100 at visible wavelengths. This is particularly pronounced for small ice crystals ($De=5$ μm). We also see that the absorption effect of soot particles is limited to wavelengths shorter than about 1.4 μm with substantially similar results in the UV and visible regions probably associated with soot optical properties; and (4) for the case of $r_{\text{soot}}=0.5$ μm, significant increases in the single-scattering co-albedo are seen especially for $De=5$ and 10 μm. In the visible, it increases from a value of $\sim 10^{-3}$ to $\sim 10^{-2}$ for contaminated ice crystals.

[11] We have also performed parameterization of the single-scattering co-albedo for external and internal mixing cases for efficient radiative forcing calculations, similar to the pure ice case except that the soot effect is included, as follows:

$$1-\varpi_0\left(\lambda, r_{\text{soot}}^{1,2}\right)=\exp\left[\sum_{n=0}^{N} b_n^*\left(\lambda, r_{\text{soot}}^{1,2}\right) De^n\right], \qquad (6)$$

$$1=\text{external mixing}, 2=\text{internal mixing},$$

where the single-scattering co-albedo ϖ_0 and fitting coefficients b_n^* are functions of the soot radius and mixing state.

3. Radiative Forcing Calculations and Analysis

[12] To investigate the radiative effect of contaminated contrail cirrus in the solar spectrum, we have used the Fu-Liou model [*Fu and Liou*, 1993; *Gu et al*., 2011] for broadband radiative transfer calculations. In this model, the correlated *k*-distribution method and the delta-four-stream approximation for flux calculations have been integrated in a coherent manner to account for spectral line absorption and multiple scattering. The solar spectrum is divided into six bands according to the locations of major absorption bands. Three sets of radiative transfer computations have been carried out, including (1) contrail cirrus with pure ice particles, (2) contaminated contrail with ice particles externally or internally mixed with a soot particle radius of 0.1 μm, and (3) contaminated cirrus externally or internally mixed with a soot particle radius of 0.5 μm. In the computations, we have used the US 1976 standard atmosphere, along with the solar constant, solar zenith angle, surface albedo, cloud base height, and cloud thickness of 1366 W/m^2, 60°, 0.1, 9.5 km, and 1 km, respectively. The solar radiative forcing and heating rate profiles were calculated for IWCs in the range of ~0.0 to 0.01 g m^{-3} and for *De* from 2 to 30 μm, which are in line with those of laboratory and field campaign studies for contrail cirrus.

[13] Cloud solar radiative forcing results for two states of soot contamination are presented with reference to the contrail cirrus ice crystal size and other pertinent parameters defined at the top of the atmosphere (TOA), surface (SFC),

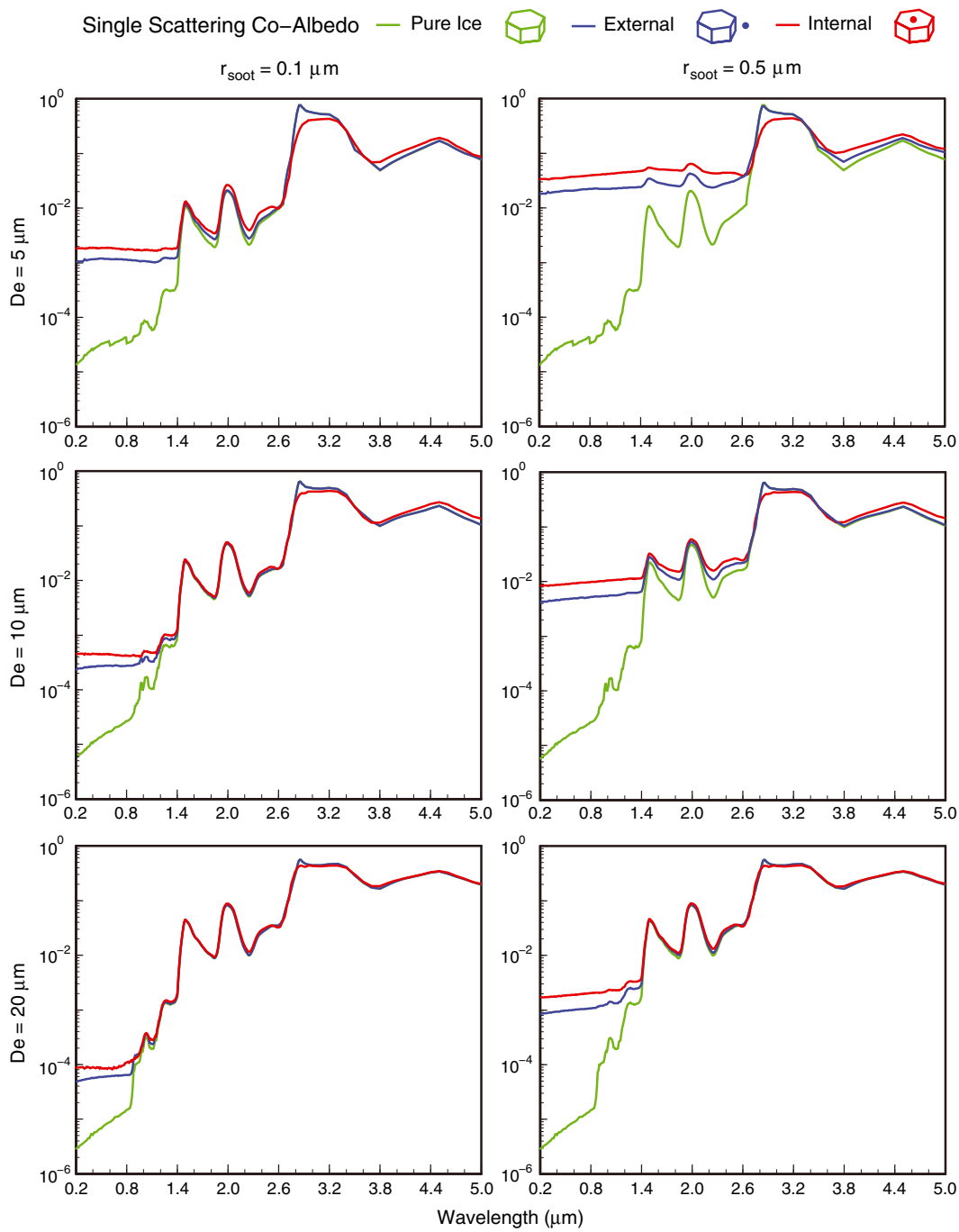

Figure 2. Spectral single-scattering co-albedo for pure ice plate and external and internal mixing cases as a function of wavelength from 0.2 to 5 µm for three mean effective ice crystal sizes of 5, 10, and 20 µm and two soot radii of 0.1 and 0.5 µm.

and within the atmosphere. Also, two visible optical depths of 0.5 and 1 were selected for illustration purposes. The cirrus optical depth is related to *De* and IWP through the parameterization denoted in equation (3). The symbol ΔF is the difference of net solar fluxes between contaminated and pure contrail cirrus at a given level, at which the net flux is defined as the difference between downward and upward fluxes. Thus, the difference between ΔF_{TOA} and ΔF_{SFC}, defined as ΔF, represents the impact of soot contamination in contrail cirrus on the column atmosphere.

[14] In Figure 3, the following general patterns are evident: (1) The radiative forcing at TOA is positive, indicating that the soot effect is to increase the absorption of solar energy within the Earth-atmosphere system. For an optically thin cloud with an optical depth of 0.5, we see a large ΔF_{TOA} of ~6 W/m^2 for $De = 5$ µm and $r_{\mathrm{soot}} = 0.5$ µm with internal mixing state, while in the case of external mixing, ΔF_{TOA} reduces by a factor of 2 (~3 W/m^2). When $r_{\mathrm{soot}} = 0.1$ µm, ΔF_{TOA} becomes quite small, with values of ~0.2 and 0.1 W/m^2 for internal and external mixing states, respectively, in the case of $\tau_{\mathrm{VIS}} = 0.5$, but these values increase to ~0.8 and 0.4 W/m^2, respectively, in the case of $\tau_{\mathrm{VIS}} = 1$. Due to the large variability of radiative forcing, values for the case $r_{\mathrm{soot}} = 0.1$ µm are small and are obtained

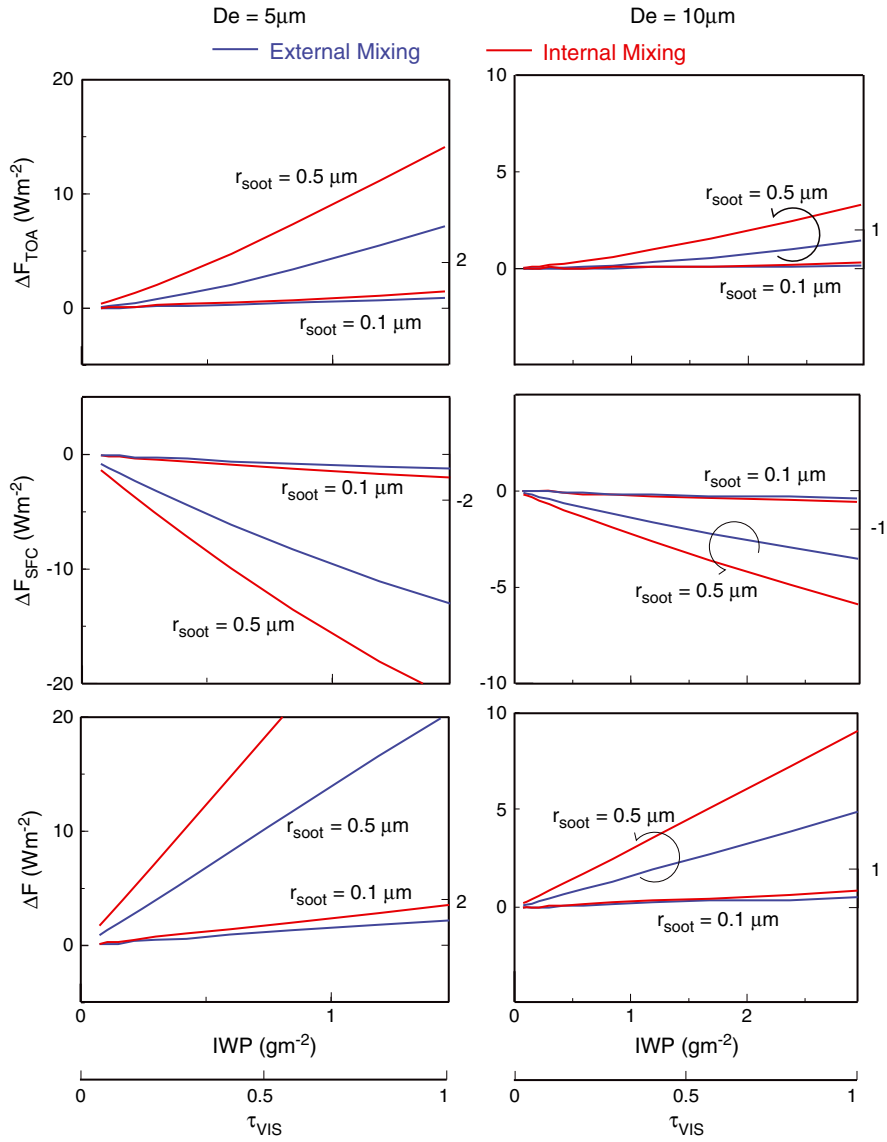

Figure 3. Radiative forcings of contrail cirrus produced by external and internal contamination of soot particles for two effective ice crystal sizes of 5 and 10 μm as a function of visible optical depths. Vertical scale for the case of 0.5 μm soot radius (left). Vertical scale for the case of 0.1 μm soot radius (right). The terms ΔF_{TOA} and ΔF_{SFC}, and ΔF (W/m^2) are radiative forcings at TOA, the surface, and within the atmosphere, respectively. All the input parameters used in the calculations are defined in the text.

from the computer output. The effect of $r_{soot} = 0.1$ μm on $De = 10$ μm reduces ΔF_{TOA} by a factor of ~10. (2) The effect of soot particles on ΔF_{SFC} depicts negative values because additional solar energy is absorbed in the atmosphere associated with soot addition; however, the magnitude of the reduction is dependent on the parameters displayed in Figure 3. (3) Lastly, the radiative forcing due to soot contamination in contrail cirrus within the atmospheric column, ΔF, i.e., difference between ΔF_{TOA} and ΔF_{SFC}, are shown in the bottom panels. Confined to the cases involving $\tau_{VIS} = 0.5$ and $De = 5$ μm, the ΔF values are ~18 and 10 W/m^2 for internal and external mixing, respectively, for $r_{soot} = 0.5$ μm. Even for $r_{soot} = 0.1$ μm, we obtain values of ~0.8 and 0.5 W/m^2 for internal and external mixing cases, respectively. We have compared the internal mixture of a single soot particle in a contrail crystal with its external mixture counterpart and have shown the critical importance of the former in radiative forcing evaluation (Figure 3). However, the results here should not be directly compared with the pure ice case. In accordance with the observed results presented by *Petzold et al.* [1998, 1999], plural numbers of soot particles inside and outside of contrail particles have been observed [see *Petzold et al.*, 1998, Figure 1, Table 4]. Multiple inclusions of soot particles larger than 0.1 μm in size will increase TOA radiative forcing and is a research area requiring further investigation (see also radiative forcing results for $r_{soot} = 0.5$ μm).

[15] Figure 4 depicts the solar heating rate profiles for four atmospheric conditions: clear (no contrail cirrus), pure ice, external mixing, and internal mixing in the height scale from 0 to 20 km with a vertical resolution of 1 km, except in the cloud layer (9.5–10.5 km), which is divided into four layers for illustration purposes. Note that the heating rate is proportional to the net flux divergence at two levels divided

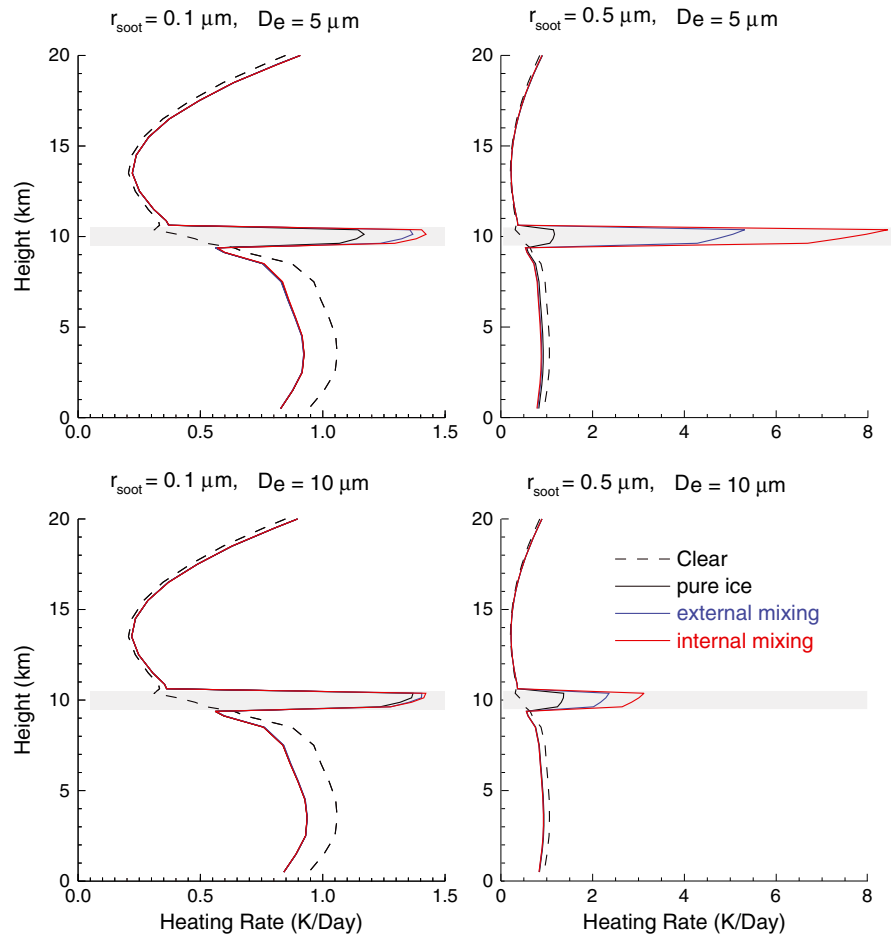

Figure 4. Instantaneous atmospheric and cloud heating rates produced by the absorption of solar radiation in clear and contrail cirrus atmospheres. The contrail cirrus contains pure and contaminated ice particles of 5 and 10 µm mean effective sizes with the latter externally and internally mixed with soot particle radii of 0.1 and 0.5 µm. The cloud is located between 9.5 and 10.5 km. All the input parameters used in the calculations are defined in the text.

by the associated thickness in cloud, and is therefore dependent on the vertical layer used in the calculations. With the atmospheric conditions and the solar constant and solar zenith angle defined previously, the instantaneous heating rate in a clear atmosphere is on the order of 0.5 to 1 K/day in the troposphere that is primarily produced by water vapor. Above 15 km, ozone picks up the heating in the stratosphere. We have used a visible optical depth of 0.5 for contrail cirrus in the heating rate presentation. Consistent with radiative forcing results, the case of internal mixing produces the largest heating rate in all contrail cirrus conditions. However, the effect is largely confined within the thin-cloud layer; heating rates above and below the cloud do not show noticeable differences between pure and contaminated cases. For the most realistic case involving $De = 5$ µm and $r_{soot} = 0.1$ µm, the cloud heating rate increases from ~1.1 K/day for pure ice to ~1.35 K/day for external mixing to ~1.4 K/day for internal mixing. A thin contrail cirrus cloud slightly increases heating above the cloud but reduces the heating by about 0.2 K/day below the cloud. For a larger *De* of 10 µm, ice absorbs more solar radiation, the soot contamination effect reduces, and the condition of external or internal mixing appears to have little consequence. For the case of $r_{soot} = 0.5$ µm, substantial cloud heating can be generated, and the mixing state effect becomes significant, as shown in the diagrams (Figure 4, right), especially for $De = 5$ µm, for which an instantaneous heating rate of ~8 K/day is shown.

4. Concluding Remarks

[16] We have conducted an analysis of the effect of internal and external contamination of ice crystals by soot particles on the single-scattering and radiative properties of contrail cirrus in the atmosphere. For baseline calculations, we have used a simple ice plate shape and two mixing states involving external mixing and internal mixing. For the single-scattering properties of pure ice crystals, the recent database developed by *Yang et al*. [2013] was employed to cover the solar spectrum from 0.2 to 5 µm for three mean effective ice crystal sizes $De = 5$, 10, and 20 µm in reference to the extinction coefficient, single-scattering co-albedo, asymmetry factor, and three additional expansion terms in the phase function. We subsequently developed the spectral parameterization of these single-scattering properties in terms of polynomial functions to achieve accuracy within 0.1%.

[17] For the calculations of the single-scattering properties for ice particles contaminated by soot, we followed the approach innovated by *Liou et al*. [2010, 2011] for the condition of external and internal mixing states assuming two soot radii of 0.1 and 0.5 μm to illustrate sensitivity on the transfer of solar radiation. The incorporation of these soot particles only impacts the single-scattering co-albedo, whereas the extinction coefficient and asymmetry factor remain essentially unchanged. The internal mixing state absorbs substantially more radiation as compared with the external mixing counterparts due to the enhancement of light absorption from all directions. The soot absorption effect is largely confined to a wavelength of about 1.4 μm, beyond which ice absorption takes over.

[18] Substantial radiative forcing values at TOA, the surface, and within the atmosphere on the order of 10 W/m^2 are shown for internal mixing states in the case of a small ice crystal size ($De = 5$ μm) and a large soot particle ($r_{soot} = 0.5$ μm). For a more realistic case of $r_{soot} = 0.1$ μm coupled with a visible cloud optical depth of 0.5, the radiative forcing at TOA is on the order of 0.2 W/m^2, while that within the atmosphere is on the order of 0.8 W/m^2 for the internal mixing case. These forcings are reduced by a factor of about 2 in the external mixing case. The absorption of solar radiation by a cloud layer leads to its heating and affects the heating rates below the layer. For the case described above, the cloud heating rate increases from about 1.1 K/day for pure ice to about 1.4 K/day for the internal mixing case. The increase in cloud heating leads to the reduction of atmospheric heating below the cloud.

[19] While we have initiated an analysis of the radiative forcings of contrail cirrus contaminated by soot particles produced by high-flying aircraft, we have made numerous approximations to simplify complex computations. For example, the plate shape assumption should be replaced by a more realistic habit distribution, and the possible combination of internal mixing followed by external mixing should also be considered in the analysis. Determination of the multiple-inclusion positions from observations and development of an appropriate light-scattering and light-absorption approach is a challenging research area requiring further investigation. Moreover, we need to search for available radiative flux observations to cross-check theoretical results. Finally, the parameterization developed in this paper involving internal and external mixing should be tested in an appropriate regional model such as the Weather Research and Forecast model for impact analysis and physical understanding.

[20] **Acknowledgments.** This research was supported by Subcontract S100034 from Texas A&M Research Foundation through the ACCRI program and by the National Science Foundation under the Grant AGS-0946315.

References

d'Almeida, G. A., P. Koepke, and E. P. Shettle (1991), Atmospheric Aerosols, DEEPACK, Hampton, VA.

Christiansen, C. (1884, 1885), Untersuchungen über die optischen Eigenschaften von fein verteilten Körpern, *Ann. Phys. Chem.*, *23*, 298–306, *24*, 439–446.

Fu, Q., and K. N. Liou (1993), Parameterization of the radiative properties of cirrus clouds, *J. Atmos. Sci.*, *50*, 2008–2025.

Gu, Y., K. N. Liou, S. C. Ou, and R. Fovell (2011), Cirrus cloud simulations using WRF with improved radiation parameterization and increased vertical resolution, *J. Geophys. Res. 116*, D06119, doi:10.1029/2010JD014574.

Iwabuchi, H., P. Yang, K. N. Liou, and P. Minnis (2012), Physical and optical properties of persistent contrails: Climatology and interpretation, *J. Geophys. Res.*, *117*, D06215, doi:10.1029/2011JD017020.

Krekov, G. M. (1993), Models of atmospheric aerosols, in Aerosol Effects on Climate, edited by S. G. Jennings, pp. 9–72, University of Arizona Press, Tucson, AZ.

Liou, K. N., Y. Gu, Q. Yue, and G. McFarguhar (2008), On the correlation between ice water content and ice crystal size and its application to radiative transfer and general circulation models, *Geophys. Res. Lett.*, *35*, L13805, doi:10.1029/2008GL033918.

Liou, K. N., Y. Takano, and P. Yang (2010), On geometric optics and surface waves for light scattering by spheres, *J. Quant. Spectrosc. Radiat. Transfer*, *111*, 1980–1989.

Liou, K. N., Y. Takano, and P. Yang (2011), Light absorption and scattering by aggregates: Application to black carbon and snow grain, *J. Quant. Spectrosc. Radiat. Transfer*, *112*, 1581–1594.

Liou, K. N., P. Yang, Y. Takano, K. Sassen, T. Charlock, and W. Arnott (1998), On the radiative properties of contrail cirrus, *Geophys. Res. Lett.*, *25*, 1161–1164.

Petzold, A., and A. Döpelheuer (1998), Reexamination of black carbon mass emission indices of a jet engine, *Aerosol Sci. Technol.*, *29*, 355–356.

Petzold, A., A. Döpelheuer, C. A. Brock, and F. P. Schröder (1999), In situ observations and model calculations of black carbon emission by aircraft at cruise altitude, *J. Geophys. Res.*, *104*, 22171–22181.

Petzold, A., J. Ström, S. Ohlsson, and F. P. Schröder (1998), Elemental composition and morphology of ice-crystal residual particles in cirrus clouds and contrails, *Atmos. Res.*, *49*, 21–34.

Schumann, U., F. Arnold, R. Busen, J. Curtius, B. Kärcher, A. Kiendler, A. Petzold, H. Schlager, F. Schröder, and K.-H. Wohlfrom (2002), Influence of fuels sulfur on the composition of aircraft exhaust plumes: The experiments SULFUR 1-7, *J. Geophys. Res.*, *107*, doi:10.1029/2001JD000813.

Ström, J., and S. Ohlsson (1998), In situ measurements of enhanced crystal number densities in cirrus clouds caused by aircraft exhaust, *J. Geophys. Res.*, *103*, 11,355–11,361, doi:10.1029/98JD00807.

Yang, P., L. Bi, B. A. Baum, K. N. Liou, G. Kattawar, M. Mishchenko, and B. Cole (2013), Spectrally consistent scattering, absorption, and polarization properties of atmospheric ice crystals at wavelengths from 0.2 to 100 μm, *J. Atmos. Sci. 70*, 330–347, doi: http://dx.doi.org/10.1175/JAS-D-12-039.1.

Yang, P., K. N. Liou, K. Wyser, and D. Mtichell (2000), Parameterization of the scattering and absorption properties of individual ice crystals, *J. Geophys. Res.*, *105*, 4699–4718.

Yang, P., H. Wei, H.-L. Huang, B. A. Baum, Y. X. Hu, G. W. Kattawar, M. I. Mishchenko, and Q. Fu (2005), Scattering and absorption property database for nonspherical ice particles in the near- through far-infrared spectral region, *Appl. Opt.*, *44*, 5512–5523.